JJEE
Volume 11 | Number 4 | Pages 743-757

Jordan Journal of Electrical Engineering

ISSN (print): 2409-9600, ISSN (online): 2409-9619

Homepage: jjee.ttu.edu.jo

Improving UWB-Based Real-Time Location Data with IMU Sensor Under NLOS Conditions

Ramazan Kavak[1,3], Serap Cekli[2]

[1] Graduate Education Institute, Istanbul University - Cerrahpasa, Istanbul, Turkiye
E-mail: ramazankavak@ogr.iuc.edu.tr
[2]Electrical and Electronics Engineering, Istanbul University - Cerrahpasa, Istanbul, Turkiye,
[3]Asis Automation and Fueling Systems Inc., R&D Center, Istanbul, Turkiye.

Received: Sep 20, 2025 *Revised: Nov 02, 2025* *Accepted: Nov 21, 2025* *Available online: Jan 20, 2026*

***Abstract*—** This study examines the degradation of known positioning data in Ultra-Wideband (UWB) Real-Time Location Systems (RTLS) under Non-Line-of-Sight (NLOS) conditions, which are frequently encountered in indoor environments (e.g., walls, metal cabinets, shelves). The Decawave DW1000, which uses Two-Way Ranging (TWR), demonstrates reliable performance in Line-of-Sight (LOS) conditions, but in NLOS conditions, multipath causes significant deviation and dispersion. To mitigate these effects, we propose an IMU-assisted fusion approach that integrates a 6-axis Inertial Measurement Unit (IMU) with the UWB pipeline. This approach reduces the NLOS positioning error by up to 89.52% compared to the baseline using UWB alone. With the proposed method, the Mahony filter is used with PID gains (K_p, K_i) tuned for real-time response; accelerometer cues detect and eliminate sudden jumps caused by multipath. The combined UWB-IMU measurements are then processed by an Extended Kalman Filter (EKF), which explicitly models the temporal dynamics and measurement uncertainty, yielding smoother and more reliable data. We evaluate the method under LOS and NLOS conditions against a baseline system using only UWB; MATLAB-based analyses confirm the stated improvement. These findings validate the effectiveness of IMU-assisted fusion for UWB-based RTLS in complex indoor environments and present a practical method for high-accuracy positioning with modest computational load and sensor complexity.

***Keywords*—** Real-time location system; Inertial measurement unit; Ultra-Wideband; Two-way ranging measurement; Extended kalman filter.

1. INTRODUCTION

Nowadays, various indoor RTLS solutions are offered using Radio Frequency Identification (RFID), Bluetooth and UWB [1]. Many features of wireless technologies are important to implement indoor positioning system in a specific application, see Fig. 1. Examples of these are: modulation type used for data transmission, power consumption of the system, channel capacity, transmission time and efficiency of the system. UWB-based communication and positioning systems have become quite popular recently. It can provide precise positioning down to centimeter level with its high multi-channel resolution [2]. In addition, high-speed data transmission can be achieved thanks to UWB. Because the limited channel capacity of narrow-band systems provides low signal quality. The system uses the DWM1000 module [3]. In this study, an approach is proposed to solve the problems encountered in NLOS situations in indoor UWB-based positioning systems. In particular, in the TWR method applied with the DWM1000 module, signal deviations due to obstacles, sudden jumps and inconsistencies in position data occur. In such cases, the integration of MEMS

* Corresponding author
DOI: https://doi.org/10.5455/jjee.204-1758400512

(Micro-Electro-Mechanical Systems) based IMU sensors into RTLS systems is increasingly used in the literature in order to increase position accuracy. In particular, the MPU6050 is an IMU sensor suitable for RTLS solutions that can be easily integrated into embedded systems with its low-cost, compact structure. Using gyroscope and accelerometer data, attitude, heading, and acceleration are estimated, and the plausibility of position measurements is assessed.

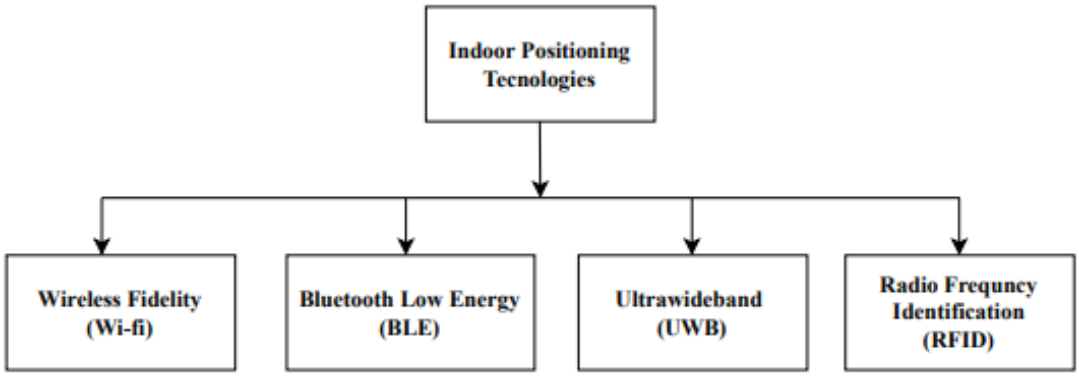

Fig. 1. Current technologies used in real-time positioning systems.

For this reason, the MPU6050-based IMU sensor has also been integrated into our system. The aim is to obtain orientation information with gyroscope data obtained from the IMU, and acceleration change information on the axes with accelerometer data. With this data, anomalies and jumps in the position data obtained with UWB signals can be determined and filtered. In addition, by combining these two data sources with the EKF algorithm, both the accuracy and stability of the system have been increased. EKF provides state estimation in nonlinear systems, especially allowing to combine the short-term sensitivity of IMU with the long-term accuracy of UWB. The developed system has been simulated in MATLAB and tested in a closed and obstructed environment with various motion scenarios. UWB data has been filtered using an IMU sensor; both sensor fusion and error correction have been performed using EKF. The results obtained show that position errors have been significantly reduced, especially in NLOS conditions.

It has been shown that IMU data and UWB data have been combined within the framework of sensor fusion and accuracy and stability have been achieved. For example; Feng et al. (2020) combined IMU and UWB data using Kalman filter and achieved high-accuracy indoor positioning [4]. Zhu et al.(2023) presented a two-stage error correction and sensor fusion model to increase positioning accuracy by considering the tight coupling of UWB and IMU data [5]. Wei et al. (2025) proposed a multi-sensor fusion localization approach based on Gaussian-Adaptive Unscented Kalman Filtering (Gauss-AUKF) to improve UWB/IMU integration accuracy by mitigating range errors and minimizing filter divergence through adaptive noise covariance updating [6]. Wang & Li et al. (2017) obtained more reliable indoor positioning results by combining UWB and IMU data using Particle Filter [7]. Zhan et al. (2024) used Unscented Kalman Filter (UKF) to provide a more linear and stable location estimation by combining IMU and UWB data with sensor fusion [8]. These articles cover significant developments in recent years regarding improving position accuracy through sensor fusion of UWB and IMU data, particularly under NLOS conditions.

In this study, UWB technology, TWR method, MEMS sensor used and EKF are mentioned under the title of Materials and Methods in Section 2. In Section 3, the proposed system and

algorithm architecture, tests and results are explained. In the last section, the test results are analyzed and suggestions are made for future studies.

2. MATERIALS AND METHODS

In our study, information about the technology used, position estimation method, proposed IMU sensor and used filter is given under the following headings respectively.

2.1. UWB

UWB-based RTLS covers a very wide frequency band. RF signals in the 500 MHz band range are used in these systems. UWB systems are based on the principle of pulse-based signal transmission, which allows them to operate at very low power levels. UWB technology can be widely used in indoor positioning applications, and the range frequency used is usually between 3.1 GHz and 10.6 GHz [9]. High bandwidth can provide high data transfer speed and high precision results even in environments with dense obstacles. High bandwidth also provides high resilience to signal attenuation, resistance to noise, and greater accuracy in range and geographic location determination [9]. UWB technology also has a high ability to pass through obstacles such as walls, wood, and clothing, but liquids and metal materials still cause signal loss. UWB-based RTLS can also be widely used for certain applications due to their approach to spectrum sharing in fixed-band environments. UWB is used in many different applications, from consumer electronics to medical electronic devices and industrial automation [10]. UWB technology is also advantageous in this regard. In UWB RTLS, the system consists of three units: Tags attached to the assets, Anchor that receives the wireless signal, and a Gateway device that processes and transmits Tag locations [10].

2.2. TWR

The location finding methods commonly used in RTLS are presented in Fig. 2 below.

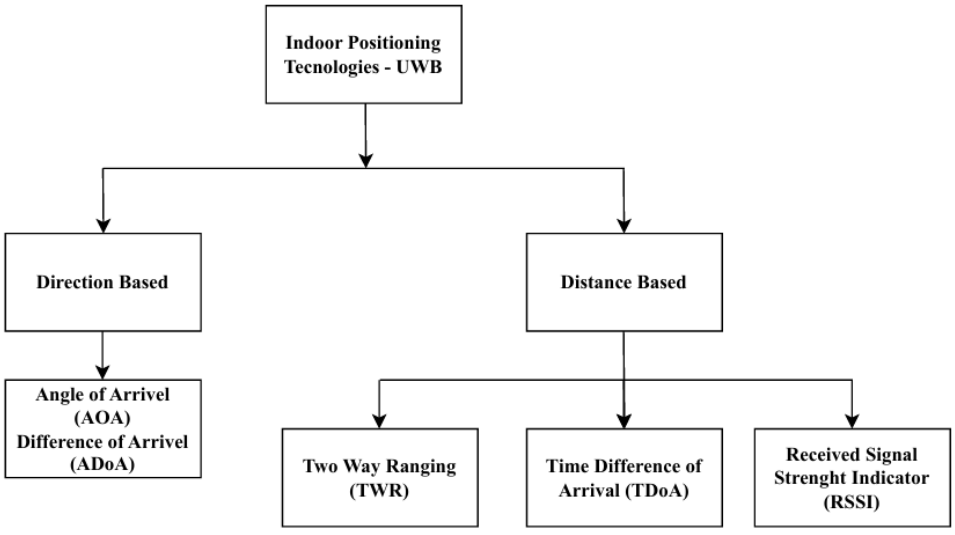

Fig. 2. Location finding methods used in RTLS.

TWR is a positioning method that estimates the distance by measuring the time of flight (ToF) between two wirelessly communicating devices [11]. This method is widely used especially in UWB systems. TWR is a cost-effective and more practical method than TDOA since it works without requiring time synchronization.

TWR is a two-way messaging method between a Tag (mobile device) and an Anchor (fixed reference point). The process generally consists of 3 stages [11], see Fig. 3:

Poll (Request): Tag sends a message to the anchor.

Response: Anchor receives the message and sends a response after a certain processing time.

Final: Tag receives the response and calculates the distance according to all time measurements.

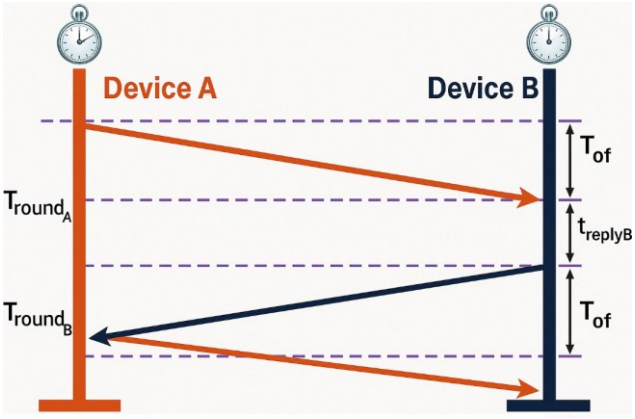

Fig. 3. Times between two devices for the TWR method [12].

$$T_{roundA} = 2 \times T_{of} + T_{replyB} \quad (1)$$

$$T_{roundB} = 2 \times T_{of} \quad (2)$$

$$T_{tof} = \frac{1}{4}\left(T_{roundA} + T_{roundB} - T_{replyB}\right) \quad (3)$$

Here [12]:

T_{roundA} : Total time from sending the first message to receiving the Anchor response, measured by Tag (mobile device).

T_{roundB} : Time from sending the response to receiving the last message, measured by Anchor (fixed device).

T_{replyB} : Processing time from the moment the Anchor device receives the incoming message until it responds.

d : Calculated distance (in meters) :

$$d = c \times T_{of} \quad (4)$$

When a fast-messaging algorithm created in TWR, a precision of up to 10 cm can achieved. A location finding method can be created with a simple algorithm such as trilateration. Some disadvantages of this method are as follows: Two-way communication is required to calculate the location. Timing problems may occur when there is a tag density. Although it provides location accuracy performance of up to 10 cm in LOS situations, there is a loss of performance due to signal reflections in NLOS situations. Again, due to two-way communication, it may have a negative effect on power consumption, especially when used with battery [13].

2.3. MEMS

The location accuracy of UWB can sometimes be affected by factors such as signal reflection. At this point, sensors that provide motion and orientation data can complement UWB data and enable more accurate and reliable location tracking. One such sensor is the

MPU6050, which is low-cost and capable of providing high data accuracy. One of these sensors is the low-cost and high-accuracy MPU6050. The MPU6050 is an integrated MEMS-based motion detection sensor. This sensor includes a 3-axis accelerometer, a 3-axis gyroscope, and a Digital Motion Processor™ (DMP) in a small box. It includes a 16-bit ADC (Analog to Digital Converter) to digitize the accelerometer and gyroscope data [14, 15, 16], see Fig. 4.

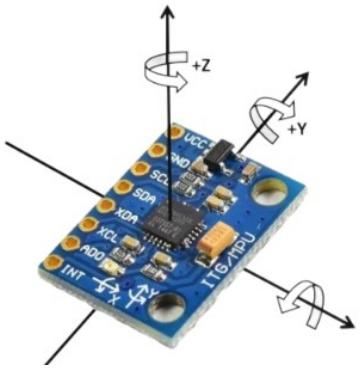

Fig. 4. MPU-6050 3-axis accelerometer and gyroscope axis reference systems [17].

The MPU6050 is typically not used stand-alone; it performs best when fused with other sensors. It can be used with RTLS like UWB and can filter out location jumps, especially in NLOS situations [18].

2.4. EKF

EKF is a Bayesian method used to estimate nonlinear systems. The EKF estimates states of nonlinear systems by linearizing the system and measurement models via Jacobians. Therefore, it is similar to the working principle of the Kalman filter. The Kalman filter is not exactly a classical filter, but rather works as an estimator [19, 20].

The main difference between EKF and the traditional Kalman Filter (KF) is how it evaluates the system model. KF assumes that both the state transitions of the system and the measurement processes are linear [21]. For truly linear systems, standard KF provides an optimal and computationally simpler solution, usually measured in FLOPs (Floating Point Operations). EKF is specifically designed for systems where one or both of these operations are nonlinear. It does this by linearizing these nonlinear functions using Jacobian matrices (derived from the Taylor series expansion) at each time step [22].

EKF works in two stages, like the classical Kalman filter: Prediction and update. EKF consists of the following sequential steps [23]:

$$\hat{x}_{k/\,k-1} \quad \text{and} \quad P_k \tag{5}$$

$$\hat{x}_{k+1|k} = f(\hat{x}_{k/k}, u_k, 0) \tag{6}$$

$$P_{k+1|k} = A_k P_{k/k} A_k^T + W_k Q_k W_k^T \tag{7}$$

$$K_k = P_{k/k-1} H_k \left(H_k P_{k/k-1} H_k^T + R_k\right)^{-1} \tag{8}$$

$$\hat{x}_{k/k} = \hat{x}_{k/k-1} + K_k\left[z_k - h_k\left(\hat{x}_{k/k-1}\right)\right] \tag{9}$$

$$P_{k/k} = (1 - K_k H_k) P_{k/k-1} \tag{10}$$

Explanations of the terms used: $\hat{x}_{k/k-1}$: The predicted situation at time k (before measurement), $\hat{x}_{k/k} = \hat{x}_{k/k-1}$:The updated status at time k (after measurement), $P_{k/k-1}$: error covariance (uncertainty) of $\hat{x}_{k/k-1}$, $P_{k/k}$: error covariance of $\hat{x}_{k/k}$, u_k : Input/command vector (in our case, IMU measurements: acceleration, gyro), A_k : Jacobian (linearization) depending on

the situation W_k : Process noise input matrix, Q_k : Process noise covariance, z_k :Measurement taken at time k, H_k : Measure the Jacobian, R_k : Measurement noise covariance, K_k : is Kalman gain.

The EKF gives an approximation of the optimum generated data. The nonlinear data of the system dynamics are manipulated by a linearized method of the nonlinear system model in the final state estimation. In order for this method to work, this linearization must be a good approximation of the nonlinear model in all the uncertainties associated with the state estimation. The process flow in these equations is given in the block diagram in Fig. 5 [24].

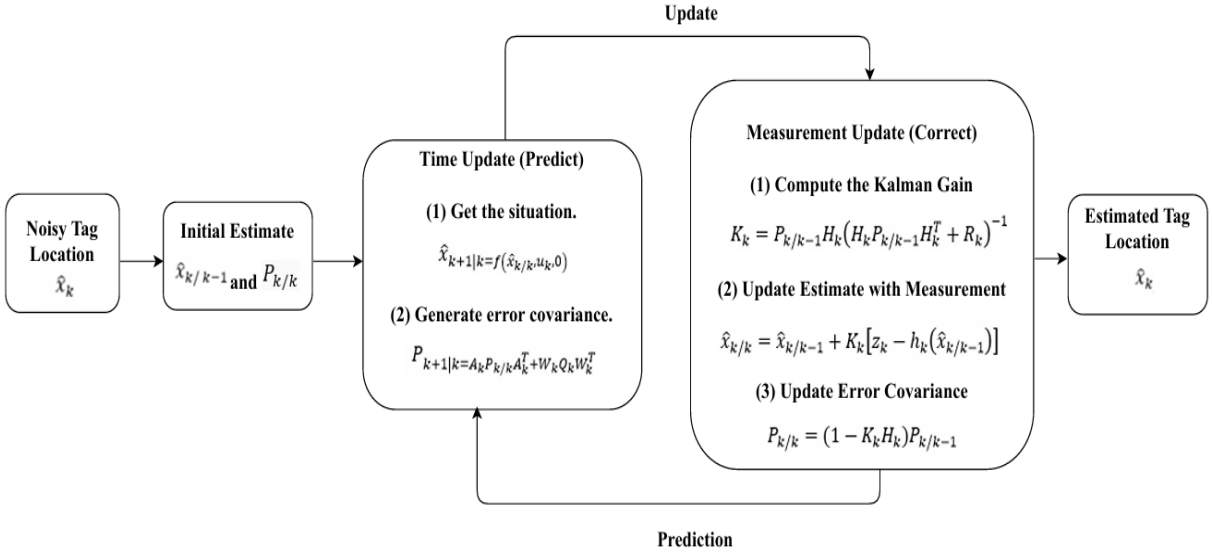

Fig. 5. Flowchart of Extended Kalman Filter.

3. INSTALLATION AND MEASUREMENT RESULTS

In the RTLS architecture we designed; 4 anchors are fixedly placed in the corners in a 25x25 m² area. A tag is placed on a moving object (human, robot, etc.). Communication between the tag and the anchors is carried out via UWB. The TWR method is used in our system. After the Tag receives the responses from the Anchors to the Poll and Final messages with the TWR method, the location data is obtained by taking the Trilateration method in 3 dimensions, see Fig. 6.

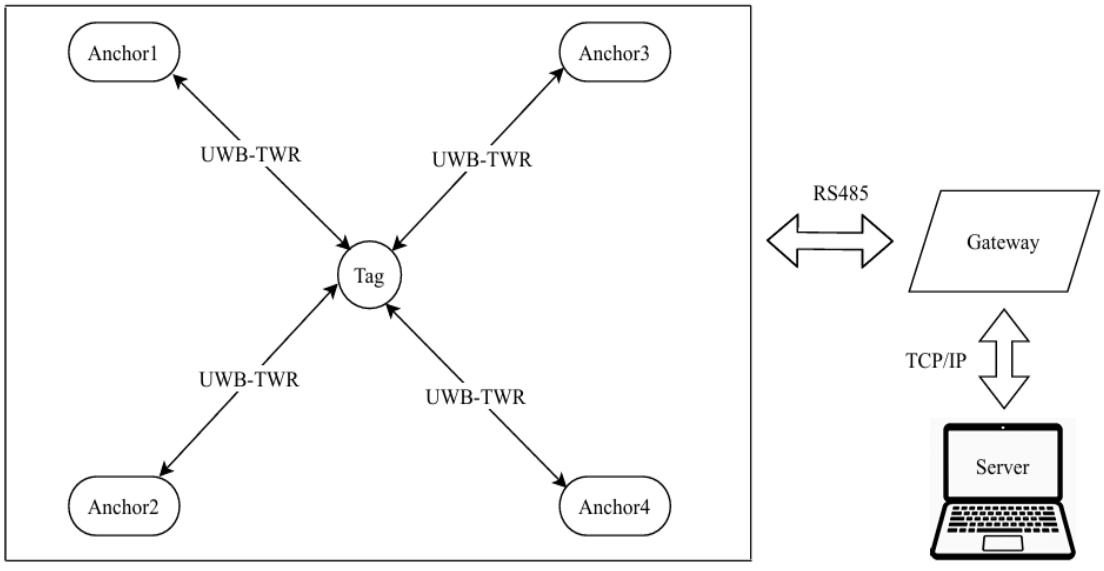

Fig. 6. Designed RTLS architecture.

Algorithm 1. IMU–assisted UWB position filtering

Input: MPU6050 (a_x, a_y, a_z, g_x, g_y, g_z), UWB TWR location (X_k, Y_k) at time k, thresholds: d_{pos} = 0.25 m, d_{acc} = 15 m/s², sample time Δ_t.
Output: Filtered position ($\hat{X}_k$, $\hat{Y}_k$) and orientation (roll, pitch, yaw). Logs saved.
// Sensor read
Wake MPU6050 (PWR_MGMT_1 ← 0), then read a_x, a_y, a_z, g_x, g_y, g_z
Read UWB preliminary location (X_{k+1}, Y_{k+1})
// Orientation (Mahony, compact)
Normalize accel; compute v from q; e ← a × v
Apply feedback (K_p, K_i) to gyro; integrate quaternion with Δ_t; normalize
Compute Euler: roll, pitch, yaw
// Acceleration deltas for gating
$\Delta A_x \leftarrow a_x(k+1) - a_x(k)$
$\Delta A_y \leftarrow a_y(k+1) - a_y(k)$
// X-axis decision
if $|X_{k+1} - X_k| > d_{pos}$ then
    if $|\Delta A_x| > d_{acc}$ then
        $\hat{X}_k \leftarrow X_{k+1}$
    else
        $\hat{X}_k \leftarrow X_k$
    end if
else
    $\hat{X}_k \leftarrow X_{k+1}$
end if
// Y-axis decision
if $|Y_{k+1} - Y_k| > d_{pos}$ then
    if $|\Delta A_y| > d_{acc}$ then
        $\hat{Y}_k \leftarrow Y_{k+1}$
    else
        $\hat{Y}_k \leftarrow Y_k$
    end if
else
    $\hat{Y}_k \leftarrow Y_{k+1}$
end if
// Logging
Save {$\hat{X}_k$, $\hat{Y}k$, a_x, a_y, a_z, roll, pitch, yaw} to record
Update state buffers: $X_k \leftarrow X_{k+1}$; $Y_k \leftarrow \hat{Y}k+1$; ax(k) ← $a_x(k+1)$; $a_y(k) \leftarrow a_y(k+1)$
return $\hat{X}_k$, $\hat{Y}_k$, roll, pitch, yaw

In our study, information about the technology used, position estimation method, proposed IMU sensor and used filter is given under the following headings respectively.

3.1. IMU Sensor Algorithm

The algorithm designed to obtain accelerometer and gyroscope data obtained using the MPU6050 IMU sensor is provided below.

Algorithm 2. Mahony-based attitude estimation (MPU-6050)

Input: Raw accelerometer $A_{xyz} = [a_x, a_y, a_z]$, raw gyroscope $G_{xyz} = [g_x, g_y, g_z]$, sample time Δ_t
Output: Quaternion q = [q0, q1, q2, q3] and Euler angles (roll, pitch, yaw).
1: //Requirements & wake-up
2: I2C write PWR_MGMT_1 ← 0
3: A_{xyz}, G_{xyz} will be read each cycle
4: //Read & calibration
5: read a_x, a_y, a_z, read g_x, g_y, g_z,
6: $A_{xyz} \leftarrow (A_{xyz} - A_{cal}[0..2]) \times A_{cal}[3..5]$
7: $G_{xyz} \leftarrow (G_{xyz} - G_{off}[0..2]) \times g_{scale}$
8: //Gravity from q and from accelerometer
9: $a_{norm} \leftarrow sqrt(a_x^2 + a_y^2 + a_z^2)$; if $a_{norm} = 0$ then skip
10: $a_x \leftarrow a_x / a_{norm}$; $a_y \leftarrow a_y / a_{norm}$; $a_z \leftarrow a_z / a_{norm}$
11: $v_x = q1 \times q3 - q0 \times q2$
12: $v_y = q0 \times q1 + q2 \times q3$
13: $v_z = q0 \times q0 - 0.5 + q3 \times q3$
14: //Error (cross product e = a × v)
15: $e_x = a_y \times v_z - a_z \times v_y$
16: $e_y = a_z \times v_x - a_x \times v_z$
17: $e_z = a_x \times v_y - a_y \times v_x$
18: //Feedback ($K_p = 25$, $K_i = 0.01$)
19: $i_x += K_i \times e_x \times \Delta_t$
20: $i_y += K_i \times e_y \times \Delta_t$
21: $i_z += K_i \times e_z \times \Delta_t$
22: $g_x \leftarrow g_x + i_x$; $g_y \leftarrow g_y + i_y$; $g_z \leftarrow g_z + i_z$
23: $g_x \leftarrow g_x + K_p \times e_x$; $g_y \leftarrow g_y + K_p \times e_y$; $g_z \leftarrow g_z + K_p \times e_z$
24: //Quaternion update (integrate gyro)
25: $q0_{old} \leftarrow q0$; $q1_{old} \leftarrow q1$; $q2_{old} \leftarrow q2$; $q3_{old} \leftarrow q3$
26: $q0 \leftarrow q0_{old} + 0.5 \times (-q1_{old} \times g_x - q2_{old} \times g_y - q3_{old} \times g_z) \times \Delta_t$
27: $q1 \leftarrow q1_{old} + 0.5 \times (q0_{old} \times g_x + q2_{old} \times g_z - q3_{old} \times g_y) \times \Delta_t$
28: $q2 \leftarrow q2_{old} + 0.5 \times (q0_{old} \times g_y - q1_{old} \times g_z + q3_{old} \times g_x) \times \Delta_t$
29: $q3 \leftarrow q3_{old} + 0.5 \times (q0_{old} \times g_z + q1_{old} \times g_y - q2_{old} \times g_x) \times \Delta_t$
30: //Normalize quaternion
31: $T_{emp} = 1.0 / sqrt(q0 \times q0 + q1 \times q1 + q2 \times q2 + q3 \times q3)$
32: $q0 \leftarrow q0 \times T_{emp}$; $q1 \leftarrow q1 \times T_{emp}$; $q2 \leftarrow q2 \times T_{emp}$; $q3 \leftarrow q3 \times T_{emp}$
33: //Euler angles
34: roll = $atan2(q0 \times q1 + q2 \times q3 , 0.5 - (q1^2 + q2^2))$
35: pitch = $asin(2.0 \times (q0 \times q2 - q1 \times q3))$
36: yaw = $-atan2(q1x\ q2 + q0 \times q3 , 0.5 - (q2^2 + q3^2))$
37: return q, roll, pitch, yaw

The skip detector combines an IMU-supported validation with a kinematic gate on inter-frame displacement. The displacement threshold,

$$\Delta p_{gate} = v_{max} \Delta t + z_\alpha \sigma_r \quad (11)$$

Here, Δt is the TWR period (500 ms), v_{max} is the expected maximum tag velocity in our experiments, σ_r is the LOS range standard deviation converted to position, and z_α = 3 (99.7% coverage area). For our Δt and motion regime, this yields a Δp_{gate} value in the 0.22–0.31 m band; the smallest value that (i) preserves > %99 of LOS samples and (ii) maximizes NLOS induced skip rejection in a delayed run has been determined to be Δp = 0.25 m. The acceleration value is obtained using the gravitational acceleration value and the accelerometer magnitude (Mahony orientation): Δa=‖a_b−g‖ is tracked, and we express this as Δa_g=Δa/ g_0 in g units; here g_0 = 9.80665 m/s². Based on the results we obtained in the tests, during the jump movement, the 99.9th percentile of Δa_g remained below 1.12–1.33 g; therefore, we set the detection threshold as Δa_g = 1.53 g (equivalent to 15 m/s²). This prevents false positive results while also allowing us to capture the sharp increases typical of multipath induced outliers. EKF covariances are adjusted using consistency-focused search (NIS matching + innovation whitening) within the range Q∈[0.005,0.05], R∈[5,15]; the selected Q=0.02, R=8 provided the best balance between accuracy and innovation consistency.

3.2. EKF Algorithm

The algorithm required to use EKF in the designed system is below.

Algorithm 3. 3D Kalman filter update

Input: state x = [x[0], x[1], x[2]], covariance P (3×3), process noise Q (3×3), measurement z = [x_{input}, y_{input}, z_{input}], measurement noise R (3×3).
Output: P, and updated (x_{input}, y_{input}, z_{input}).
1: // Step 1: Prioritization (prediction)
2: for i = 0..2 do
3: x_{pred}[i] ← x[i]
4: end for
5: for i = 0..2 do
6: for j = 0..2 do
7: P_{pred}[i][j] ← P[i][j] + Q[i][j]
8: end for
9: end for
10: // Step 2: Calculating Kalman Gain (H = I, element-wise)
11: for i = 0..2 do
12: for j = 0..2 do
13: K[i][j] ← P_{pred}[i][j] / (P_{pred}[i][j] + R[i][j])
14: end for
15: end for
16: // Step 3: Measurement update
17: y[0] ← x_{input} − x_{pred}[0]
18: y[1] ← y_{input} − x_{pred}[1]
19: y[2] ← z_{input} − x_{pred}[2]
20: for i = 0..2 do
21: x[i] ← x_{pred}[i] + K[i][i] x y[i]
22: end for
23: for i = 0..2 do
24: for j = 0..2 do
25: P[i][j] ← (1 − K[i][j]) x P_{pred}[i][j]
26: end for
27: end for
28: // Step 4: Save filtered results

29: $x_{input} \leftarrow x[0]$; $y_{input} \leftarrow x[1]$; $z_{input} \leftarrow x[2]$
30: return P, x_{input}, y_{input}, z_{input}

3.3. System Installation

In the test scenario, numerous columns and metal obstacles (metal shelves, ventilation pipes) were used in the test environment to simulate NLOS conditions. Four anchors were placed at the corners of the test environment. Tests were conducted using one Tag along the specified route. In the tests, the Tag's TWR communication time was set to 500 ms. As shown in Fig. 7, route number 1 was followed from the lower left corner. The route passed around the wall columns and through the intermediate areas. The wall columns were intended to create an NLOS effect on the UWB signals. The route was completed at the top left corner. Then, starting from the top left corner, route 2 was followed and completed upon returning to the starting point. In this test scenario, sudden maneuvers were performed around the columns, and the goal was to obtain position jumps caused by signal reflections.

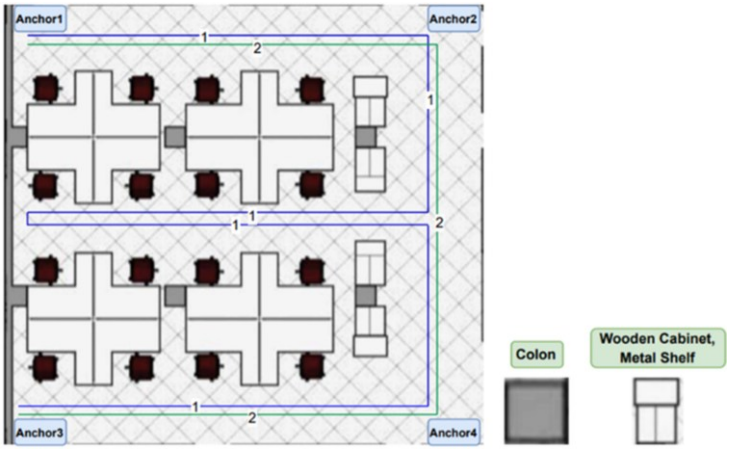

Fig. 7. The environment and test scenario created in the office for RTLS tests for the NLOS condition.

As a result of the tests conducted, as seen in Fig. 8(a), without the use of any filter algorithm, position jumps of approximately 210 cm occurred due to wall columns, wooden and metal shelves. Signal reflections occurred during sudden turning movements around wall columns and shelves. Errors in the position data are clearly visible in Fig. 8(a). Examining Fig. 8(b), we can see that the EKF applied to the system has a positive effect on the position data results. Nevertheless, errors reaching 55-60 cm occurred in the position data results obtained around wall columns and shelves. As seen in Fig. 8(c), there have been noticeable improvements in system performance with the IMU sensor algorithm we proposed for the system. Position errors caused by the effects of NLOS conditions have been reduced to an average of 22 cm. For the area defined for the LOS condition, a route has been determined as shown in Fig. 9, taking into account the area where movement can be performed.

As a result of the tests conducted, as shown in Fig. 10, the position data outputs of the system equipped with the IMU + EKF filter algorithm are more stable. Additionally, the position data shifts are less compared to a scenario without a filter. In the last scenario, the Tag is stationary and the location data obtained from the Tag for 4.5 - 5 minutes is created.

As seen in Fig. 11 for the test conducted in this scenario; when the EKF + IMU sensor algorithm was included, the location data was obtained with almost 20 cm precision.

However, in the absence of any filter, location data was obtained in the range of 20 - 60 cm circle diameter.

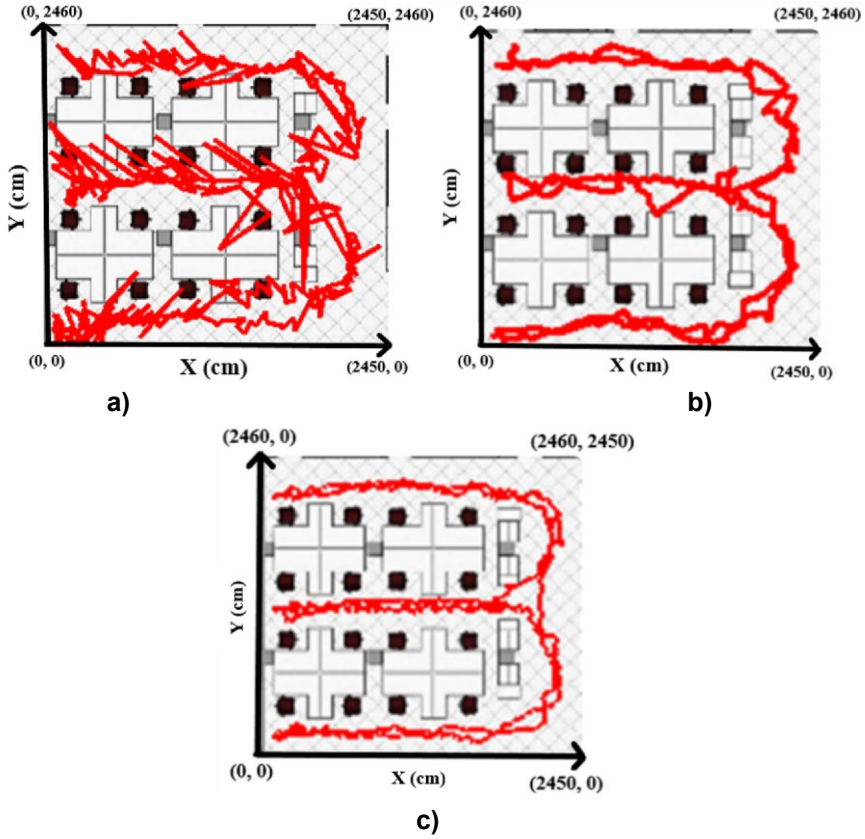

Fig. 8. Scenario test results for the NLOS environment: a) When there is no filter algorithm; b) When only EKF is in the system; c) When EKF + IMU sensor is included in the system.

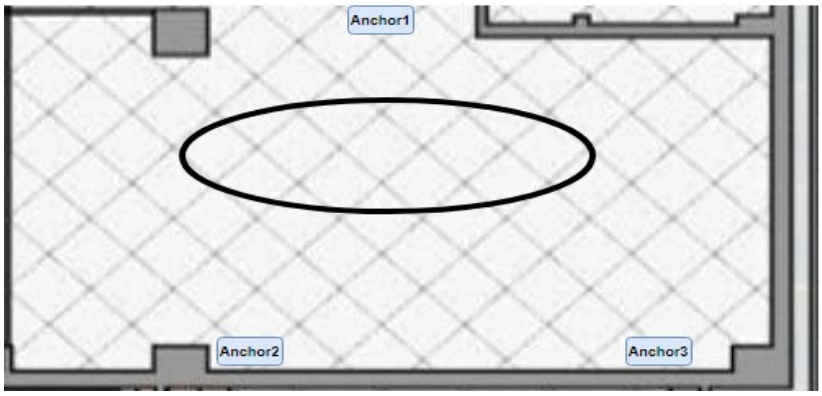

Fig. 9. Environment and test scenario created in the office for RTLS tests for the LOS condition.

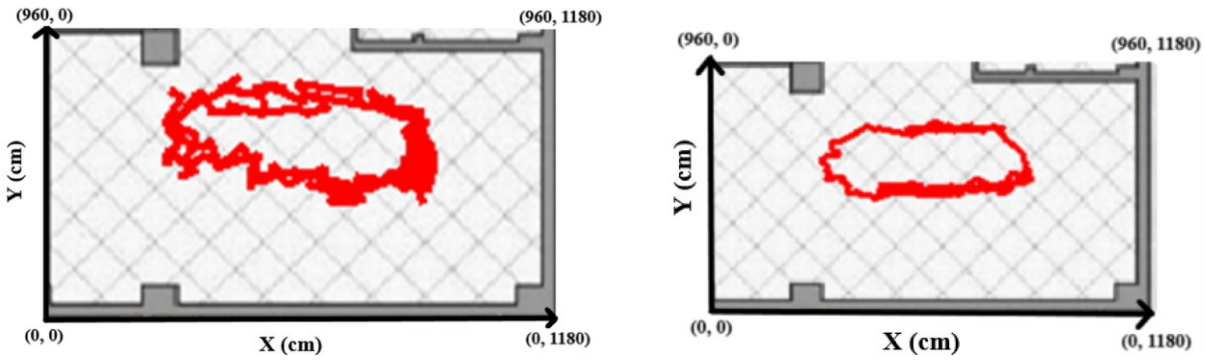

a) **b)**

Fig. 10. Scenario test results for the LOS environment: a) The situation without any filter algorithm; b) The result obtained when the EKF + IMU sensor is included in the system.

For time alignment, if the estimated position p_t=[x_t, y_t] and the actual position $p_t^\star$ = [$x_t^\star$, $y_t^\star$] are at the same time;

Error magnitude per sample:

$$e_t = \|p_t - p_t^\star\|^2 = \sqrt{(x_t - x_t^\star)^2 + (y_t - y_t^\star)^2} \quad (12)$$

$$RMSE = \sqrt{\left(\frac{1}{T}\right)\Sigma_{\{t=1\}}^{T} e_t^2} \quad (13)$$

$$\%\, Improvement = 100 \times \left(1 - \frac{RMSE_{proposed}}{RMSE_{baseline}}\right) \quad (14)$$

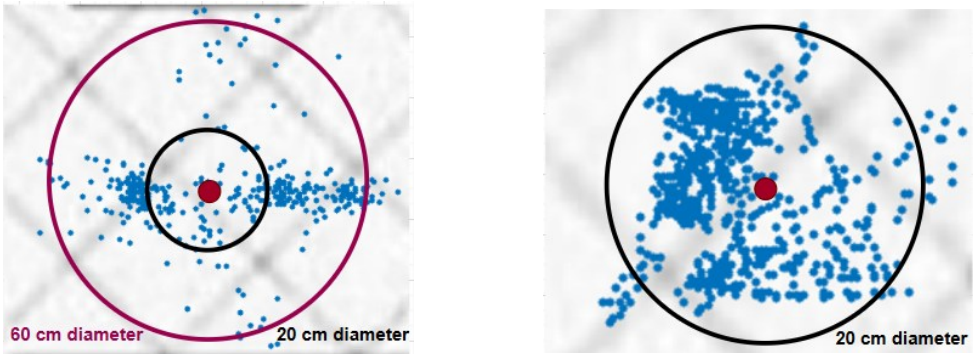

a) **b)**

Fig. 11. Location data obtained when the tag is not moving (stationary): a) The situation when there is no filter algorithm; b) The result obtained when only EKF + IMU is in the system.

Table 1. Evaluation of location data obtained under different conditions and test scenarios.

Scenario	Baseline RMSE [cm]	Proposed RMSE [cm]	% Improvement (RMSE)
NLOS	210	22	89.52
LOS	20	11	45
Sudden Direction Changes	180	26	85.56
Static Tag Condition	25	8	68

In addition to UWB data, the method we propose, which utilizes IMU sensor fusion and EKF, has reduced positioning error to approximately 22 cm under NLOS conditions. In contrast, Fan Jiang et al. (2024) reported an average error of 30 cm using UWB TWR + IMU sensor fusion [24].

Under LOS conditions, the proposed method, with the integration of IMU data, achieved an average positioning error of 11 cm. Zhu et al. (2023) reported a maximum positioning deviation of 23 cm, indicating a relatively higher variance in the accuracy of their system under comparable conditions [25].

4. CONCLUSIONS

In this study, TWR measurements are combined with MPU6050 inertial data. A lightweight, real-time hybrid UWB–IMU system is proposed using an EKF specifically designed to process NLOS-derived data. Compared to the baseline model using only UWB, this approach provides consistent gains in LOS/NLOS and static/dynamic trials. It improved position data by 89.52% while maintaining real-time operation on embedded hardware.

This study was conducted in a single enclosed space with a limited area of 25 × 25 m² and a fixed connection geometry; the results may not be directly transferable to larger or structurally different areas. However, by increasing the number of anchor points and placing the anchors according to the orthogonal array architecture, similar performance can be achieved in larger areas as well. A single tag and a fixed number of anchors were used in the experiments; multi-tag interference, congestion, and timing were not investigated. The EKF and threshold parameters were tuned for this specific area, and cross-area generalization was not evaluated. The analysis is partially based on offline MATLAB tools. Finally, the system targets 2D TWR, as measurements were taken while keeping the tag height (z-axis) constant.

Additionally, IMU drift, particularly gyro drift, can gradually affect orientation; in this work, Mahony filtering and motion-based filtering methods were used instead of open-loop drift conditions, which may allow for future drift-improved EKFs and zero-velocity updates. UWB–IMU synchronization was achieved using software time stamps and interpolation; residual vibration can affect fast motion and can be reduced using hardware time stamping or open time shift estimation.

For future work, 3D positioning tests with a non-fixed z-axis tag are planned. These tests aim to extend the system to support multiple Tags and Link Points in broader application areas. Furthermore, system performance is environment-dependent; materials, layout, and antenna placement shape NLOS. System performance can be further improved by incorporating machine learning-based signal classification techniques. For practical use in industrial and robotic applications, further optimization is foreseeable in terms of energy efficiency, system latency, and real-time decision-making performance.

Acknowledgement: The authors would like to thank R&D Center of Asis Automation and Fueling Systems Inc. for the test environment, technical support they provided during the realization of this study. Thanks for their support, for having opportunity to carry out this research.

REFERENCES

[1] A. Beauvisage, K. Ahiska, N. Aouf, "Robust multispectral visual-inertial navigation with visual odometry failure recovery," *IEEE Transactions on Intelligent Transportation Systems*, vol. 23, no. 7, pp. 9089–9101, Jul. 2022, doi: 10.1109/TITS.2021.3090675.

[2] H. Hashim, M. Abouheaf, M. Abido, "Geometric stochastic filter with guaranteed performance for autonomous navigation based on IMU and feature sensor fusion," *Control Engineering Practice*, vol. 116, p. 104926, 2021, doi: 10.1016/j.conengprac.2021.104926.

[3] Symmetry Electronics, "An overview of DecaWave's DW1000 UWB wireless transceiver for precise indoor positioning," 2024, https://www.symmetryelectronics.com/blog/an-overview-of-decawave-s-dw1000-uwb-wireless-transceiver/.

[4] D. Feng, C. Wang, C. He, Y. Zhuang, X. Xia, "Kalman filter-based integration of IMU and UWB for high-accuracy indoor positioning and navigation," *IEEE Internet of Things Journal*, vol. 7, no. 4, pp. 3133–3146, 2020, doi: 10.1109/JIOT.2020.2965115.

[5] W. Zhu, R. Zhao, H. Zhang, J. Lu, Z. Zhang, B. Wei, Y. Fan, "Improved indoor positioning model based on UWB/IMU tight combination with double-loop cumulative error estimation," *Sensors*, vol. 23, no. 3, pp. 1234–1245, 2023, doi: 10.3390/app131810046.

[6] M. Wei, L. Liu , L. Shidang, D. Wang, W. Li, "Gauss-AUKF based UWB/IMU fusion localization approach," *Ad Hoc Networks*, vol. 175, p. 103855, 2025, doi: 10.1016/j.adhoc.2025.103855.

[7] Y. Wang, X. Li, "The IMU/UWB fusion positioning algorithm based on a particle filter," *ISPRS International Journal of Geo-Information*, vol. 6, no. 8, p. 235, 2017, doi: 10.3390/ijgi6080235.

[8] H. Zhan, T. Gao, Y. Liu, Y. You, G. Wu, "Indoor pedestrian fusion localization algorithm based on unscented Kalman filter for UWB/PDR," Fourth International Conference on Sensors and Information Technology, 2024, doi: 10.1117/12.3029099

[9] Qorvo, "Getting back to basics with ultra-wideband (UWB)," 2024, https://www.qorvo.com/resources/d/qorvo-getting-back-to-basics-with-ultra-widebanduwb-white-paper.

[10] C. Lee, C. Ip, T. Park, S. Chung, "A Bluetooth location-based indoor positioning system for asset tracking in warehouse," IEEE International Conference on Industrial Engineering and Engineering Management, 2019, doi: 10.1109/IEEM44572.2019.8978639.

[11] M. Qian, K. Zhao, B. Li, A. Seneviratne, "An overview of ultra-wideband technology and performance analysis of UWB-TWR in simulation and real environment," *Indoor Positioning*, vol. 12, pp. 1–16, 2022.

[12] C. Lian, M. Adams, T. Hörmann, M. Hesse, M. Porrmann, U. Rückert, "Numerical and experimental evaluation of error estimation for two-way ranging methods," *Sensors*, vol. 19, p. 616, 2019, doi: 10.3390/s19030616

[13] M. Birem, K. Geebelen, E. Hostens, A. Mishra, J. Steckel, "Improving the accuracy and robustness of ultrawideband localization through sensor fusion and outlier detection," *IEEE Robotics & Automation Magazine*, vol. 5, no. 1, pp. 32–39, 2020, doi: 10.1109/LRA.2019.2943821.

[14] J. Liu, J. Pu, L. Sun, Z. He, "Robust IMU/UWB integration for indoor pedestrian navigation," *Sensors*, vol. 19, no. 4, p. 950, 2019, doi: 10.3390/s19040950.

[15] A. Albarbar, S. Teay, "MEMS accelerometers: Testing and practical approach for smart sensing and machinery diagnostics," *Journal of Civil Structural Health Monitoring*, vol. 7, no. 4, pp. 555–566, 2016, doi: 10.1007/978-3-319-32180-6_2..

[16] Electronic Cats, "MPU6050 Documentation," 2024, https://github.com/ElectronicCats/mpu6050/wiki.

[17] A. Abdallah, C. Chen, M. Seo, S. Kia, Z. Kassas, "PINDOC: Pedestrian indoor navigation system integrating deterministic, opportunistic, and cooperative functionalities," *IEEE Sensors Journal*, vol. 14, pp. 14424–14435, 2022, doi: 10.1109/JSEN.2022.3183887.

[18] P. Karfakis, M. Couceiro, D. Portugal, R. Cortesão, "UWB aided mobile robot localization with neural networks and the EKF," IEEE International Conference on Systems, Man, and Cybernetics, pp. 93–99, 2022, doi: 10.1109/SMC53654.2022.9945357.

[19] G. Zhou, J. Luo, S. Xu, S. Zhang, S. Meng, K. Xiang "An EKF-based multiple data fusion for mobile robot indoor localization," *Assembly Automation*, vol. 41, pp. 274–282, 2021, doi: 10.1108/AA-12-2020-0199.

[20] A. Benini, A. Mancini, S. Longhi, "An IMU/UWB/vision-based extended Kalman filter for mini-UAV localization in indoor environment using 802.15.4a wireless sensor network," *Journal of Intelligent & Robotic Systems*, vol. 70, pp. 461–476, 2013, doi: 10.1007/s10846-012-9742-1.

[21] X. Chen, Y. Xu, "Improving ultrasonic-based seamless navigation for indoor mobile robots utilizing EKF and LS-SVM," *Measurement*, vol. 92, pp. 243–251, 2016, doi: 10.1016/j.measurement.2016.06.025

[22] F. Ramirez-Echeverria, A. Sarr, Y. Shmaliy, "Optimal memory for discrete-time FIR filters in state-space," *IEEE Transactions on Signal Processing*, vol. 62, no. 2, pp. 557–561, 2014, doi: 10.1109/TSP.2013.2290504

[23] H. Chen, W. Bo, "Collaborative multiple UAVs navigation with GPS/INS/UWB jammers using sigma point belief propagation," *IEEE Access*, vol. 8, pp. 193695–193707, 2020, doi: 10.1109/ACCESS.2020.3031605.

[24] F. Jiang, D. Caruso, A. Dhekne, Q. Qu, J. Engel, J. Dong, "Robust indoor localization with ranging–IMU fusion," IEEE International Confernce on Robotics and Automation, 2024, doi: 10.1109/ICRA57147.2024.10611274.

[25] W. Zhu, R. Zhao, H. Zhang, J. Lu, Z. Zhang, B. Wei, Y. Fan, "Improved indoor positioning model based on UWB/IMU tight combination with double-loop cumulative error estimation," *Applied Sciences*, vol. 13, no. 18, p. 10046, 2023, doi: 10.3390/app131810046.